
CHEERS🍷: DECOUPLING PATCH DETAILS FROM SEMANTIC REPRESENTATIONS ENABLES UNIFIED MULTIMODAL COMPREHENSION AND GENERATION

Yichen Zhang^{1*} Da Peng^{2*} Zonghao Guo^{1†} Zijian Zhang³ Xuesong Yang³
 Tong Sun³ Shichu Sun³ Yidan Zhang³ Yanghao Li¹ Haiyan Zhao¹ Wang Xu¹
 Qi Shi¹ Yangang Sun¹ Chi Chen¹ Shuo Wang¹ Yukun Yan¹ Xu Han¹
 Qiang Ma¹ Wei Ke² Liang Wang³ Zhiyuan Liu¹ Maosong Sun¹

¹Tsinghua University ²Xi'an Jiaotong University ³University of Chinese Academy of Sciences
 yichen0zhang@gmail.com guozonghao96@outlook.com metapda@gmail.com

🤗 <https://huggingface.co/ai9stars/Cheers> 🐙 <https://github.com/AI9Stars/Cheers>

ABSTRACT

A recent cutting-edge topic in multimodal modeling is to unify visual comprehension and generation within a single model. However, the two tasks demand mismatched decoding regimes and visual representations, making it non-trivial to jointly optimize within a shared feature space. In this work, we present CHEERS, a unified multimodal model that decouples patch-level details from semantic representations, thereby stabilizing semantics for multimodal understanding and improving fidelity for image generation via gated detail residuals. CHEERS includes three key components: (i) a unified vision tokenizer that encodes and compresses image latent states into semantic tokens for efficient LLM conditioning, (ii) an LLM-based Transformer that unifies autoregressive decoding for text generation and diffusion decoding for image generation, and (iii) a cascaded flow matching head that decodes visual semantics first and then injects semantically gated detail residuals from the vision tokenizer to refine high-frequency content. Experiments on popular benchmarks demonstrate that CHEERS matches or surpasses advanced UMMs in both visual understanding and generation. Notably, CHEERS outperforms the Tar-1.5B on the popular benchmarks GenEval and MMBench, while requiring only 20% of the training cost, indicating effective and efficient (i.e., 4× token compression) unified multimodal modeling. We will release all code and data for future research.

Keywords Unified multimodal model · Visual generation and comprehension · Unified vision encoder.

1 Introduction

Multimodal large language models (MLLMs) [1, 2, 3, 4] have largely matured for visual comprehension, while diffusion models [5, 6, 7, 8, 9, 10] have set the standard for high-fidelity image generation. Bringing both into a single model is a cutting-edge step toward more human-like multimodal intelligence. However, such unification is particularly challenging, as the two tasks demand fundamentally different decoding mechanisms and visual representations.

In terms of decoding mechanisms, discretizing visual representations [11, 12, 13, 14] for autoregressive (AR) prediction with text tokens offers a seamless adaptation to existing MLLM architectures [15, 16, 17]. However, discrete tokens suffer from quantization errors [18, 19] and dimensional constraints [20, 15, 18], leading to the loss of visual information. Bypassing the constraints of sequential raster-scanning of image generation, recent approaches [21, 22, 23] integrate diffusion modeling to capture global visual context alongside AR-based text generation.

*Equal contribution.

†Corresponding author.

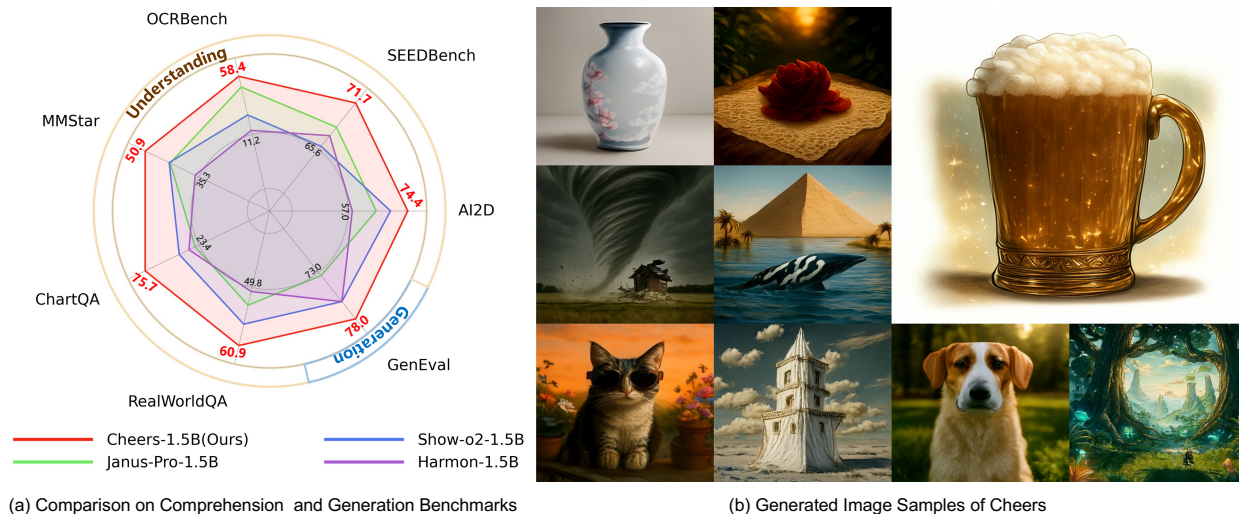


Figure 1: CHEERS Capabilities. (a) Performance on general understanding and generation benchmarks compared with unified multimodal models (UMMs) of similar scale. (b) Generated image samples of CHEERS.

From the perspective of visual representations, multimodal understanding typically relies on semantic-rich features from vision encoders [24, 25], whereas high-fidelity image generation often depends on detail-preserving latents from reconstruction-oriented tokenizers [26, 11, 27]. However, relying solely on a single representation often fails to simultaneously satisfy these distinct requirements [28, 29, 30, 31, 32, 18, 33], as shown in fig. 2 (b). Therefore, one line of UMMs [23, 34, 35] separates the feature optimization for visual comprehension and generation, achieving strong task-specific performance, as shown in fig. 2 (a). The other line seeks to integrate these capabilities via a unified token interface by either fusing heterogeneous features [21, 36] or jointly optimizing a shared vision tokenizer with multiple objectives [37, 38, 39, 40], as shown in fig. 2 (c).

Despite these inspiring explorations, the intrinsic optimization conflict between visual comprehension and generation remains insufficiently investigated in UMMs. In this paper, we introduce CHEERS, a UMM that decouples patch-level details from semantic representations, stabilizing semantics for image understanding and improving generation fidelity by injecting high-frequency detail residuals, as shown in fig. 2 (d). CHEERS includes three key components. (i) A unified vision tokenizer utilizes a representation encoder (e.g., SigLIP2-ViT) upon VAE latents to extract semantic features, subsequently compressed via a pixel-unshuffle [2] operation for efficient LLM conditioning. (ii) An LLM-based Transformer integrates autoregressive and diffusion decoding for text and image generation, respectively, thereby capitalizing on the superior modeling paradigms inherent to each modality. (iii) At the core of CHEERS is a cascaded flow matching head that explicitly decouples image generation into two phases: it initially synthesizes high-level semantics at a low resolution, followed by injecting semantically gated high-frequency residuals from the vision tokenizer to achieve precise super-resolution generation. This is akin to painting, where global structure precedes fine-grained detailing, a perspective that resonates with recent work [41].

Extensive experiments on standard benchmarks demonstrate that CHEERS performs on par with or exceeds state-of-the-art UMMs in both visual comprehension and generation, validating the efficacy of our unified modeling approach. CHEERS also represents a significant step towards token-compressed UMMs, achieving a $4\times$ compression rate for efficient high-resolution image understanding and generation. Notably, CHEERS outperforms the Tar model on the popular benchmarks GenEval and MMBench, while requiring only 20% of the training cost, indicating effective and efficient unified multimodal modeling.

Our contribution can be summarized as threefold. (1) We propose decoupling patch details from semantic representations, which redefine the multimodal feature modeling trajectory of UMMs, alleviating the optimization interference between comprehension and generation tasks. (2) We introduce CHEERS, a hybrid-decoding UMM equipped with a unified vision tokenizer that achieves significant token compression for efficient multimodal modeling. (3) We perform extensive evaluations on popular benchmarks to verify the effectiveness of CHEERS, providing detailed analysis and insights for future research.

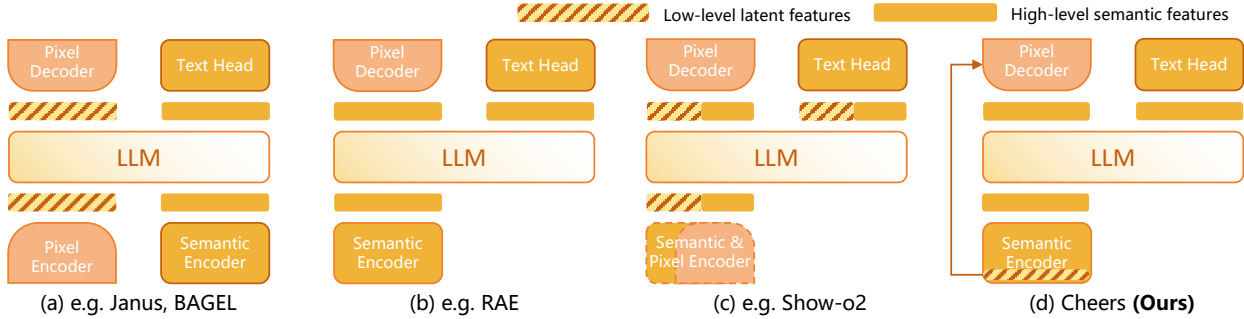


Figure 2: Architectural comparison between prior UMMs and CHEERS. (a) Separated visual spaces for understanding and generation. (b) Single semantic-centric space with limited structural details. (c) Fused feature representation with potential interference. (d) Cheers (Ours): A unified vision tokenizer that integrates structural and semantic features to ensure stable semantic understanding while enhancing generative details.

2 CHEERS 🍺

We present the CHEERS framework, covering its architecture (section 2.1), inference strategy and objectives (section 2.2), and training pipeline (section 2.3).

2.1 Model Architecture

As illustrated in fig. 3, CHEERS is built upon three key components: a unified vision tokenizer for visual encoding, a unified LLM-based Transformer backbone for multimodal modeling, and a cascaded flow matching head for image generation. Additionally, a standard text tokenizer and a language modeling (LM) head are employed for language encoding and text generation, respectively, to support visual understanding tasks.

Unified Vision Tokenizer. As illustrated in fig. 3, CHEERS adopts a unified vision tokenizer composed of a VAE decoder [6] and a semantic encoder, i.e., SigLIP2-ViT [25]. Specifically, the latent representations produced by the VAE encoder are first decoded into the image space via the VAE decoder, after which SigLIP2 extracts high-level semantic visual features. In this way, the VAE decoder and SigLIP2 jointly function as an integrated module that bridges latent representations and unified semantic visual embeddings.

Specifically, given an input image $\mathbf{X} \in \mathbb{R}^{H \times W \times 3}$, where H and W denote the image height and width, we first process it through a VAE encoder, yielding the latent states $\mathbf{z}_1 \in \mathbb{R}^{h \times w \times d}$, where $h = H/16$, $w = W/16$, and d represents the latent feature dimension. To unify diverse tasks, we formulate a task-dependent latent $\mathbf{z}_t = t\mathbf{z}_1 + (1-t)\mathbf{z}_0$, where latent noise $\mathbf{z}_0 \sim \mathcal{N}(0, 1)$. We sample timestep $t \in (0, 1)$ for image generation, fix $t = 1$ (i.e., $\mathbf{z}_t = \mathbf{z}_1$) for visual understanding, and set $t = 0$ (i.e., $\mathbf{z}_t = \mathbf{z}_0$) for language-only tasks. Subsequently, instead of directly processing these latent states \mathbf{z}_t using a ViT with randomly initialized patch embeddings like [22, 21], \mathbf{z}_t is passed through a VAE decoder $D(\cdot)$ to reconstruct the pixel-level image. The reconstructed image is then encoded by the ViT backbone to extract high-level semantic tokens $\mathbf{z}_s^{(t)} \in \mathbb{R}^{h \times w \times d'}$, where d' denotes the semantic feature dimension. To ensure strict spatial alignment between these semantic tokens and the latent patches, we adopt SigLIP2-ViT with a 16×16 patch embedding layer $S(\cdot)$. Notably, we experimentally found that direct latent processing like [22] discards fine-grained features and hinders OCR-centric understanding ability. By reconstructing the pixel space, we circumvent this issue and successfully retain essential visual details. Please kindly refer to the Supplement for details.

Before feeding the semantic tokens into our unified LLM-based Transformer, a Pixel-Unshuffle module [2] is applied to reduce their spatial resolution and project the channel dimension, resulting in $\mathbf{Z}_s^{(t)} \in \mathbb{R}^{h/2 \times w/2 \times c}$, where c is the LLM hidden size. To the best of our knowledge, we are the first work to introduce 2D token compression within a UMM.

Unified LLM-based Transformer. To achieve optimal image-text joint modeling, we utilize autoregressive decoding for text generation and diffusion processes for image generation within a single LLM backbone, i.e., Qwen2.5-1.5B-Instruct [42]. Specifically, given the semantic visual tokens $\mathbf{Z}_s^{(t)}$ and the text embeddings \mathbf{Z}_{text} derived from input instructions via the text tokenizer, we concatenate them into a unified input sequence, which is then processed by the LLM backbone to yield contextualized hidden states through deep cross-modal encoding. Note that a bidirectional attention mask is applied to $\mathbf{Z}_s^{(t)}$ to capture global visual context, whereas a causal mask is employed for \mathbf{Z}_{text} to

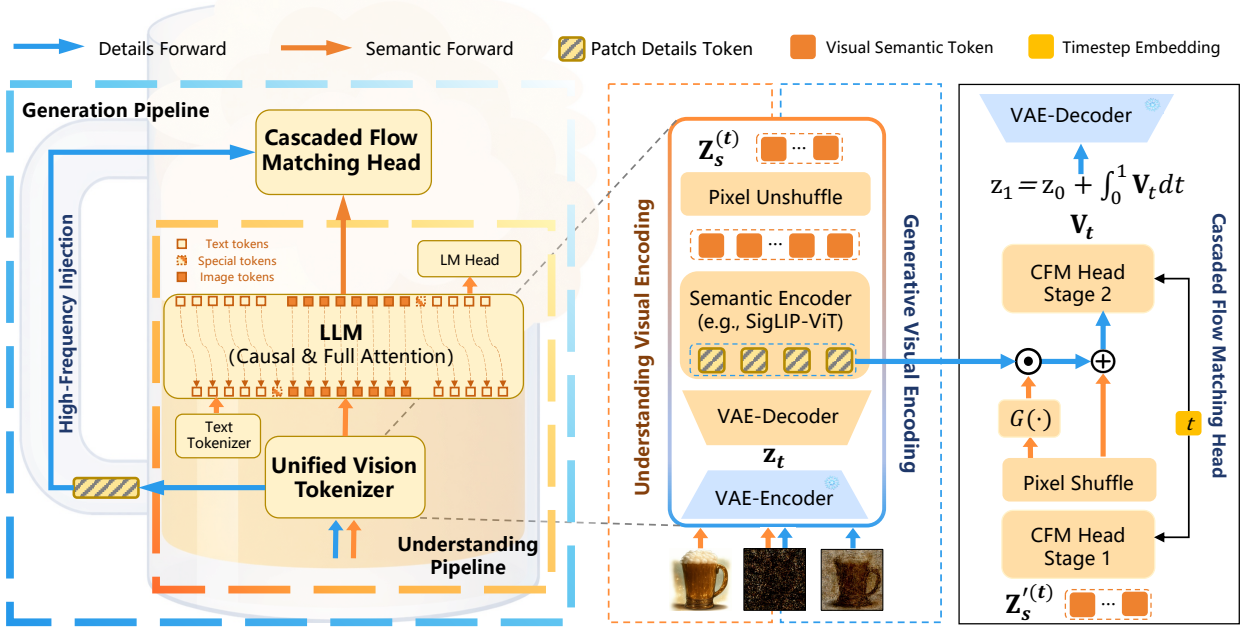


Figure 3: Overview of CHEERS, a unified framework for multimodal understanding and image generation. The Unified Vision Tokenizer converts visual inputs into semantic tokens that are jointly processed with text tokens by the LLM for understanding tasks, and detail tokens that serve as step-adaptive high-frequency injection into the CFM Head during generation. During generation, the CFM Head predicts a continuous-time velocity field in the latent space, enabling iterative sampling from Gaussian noise \mathbf{z}_0 to the terminal latent \mathbf{z}_1 , which is finally decoded by the VAE decoder.

enable AR decoding. Depending on the task modality, the LLM outputs are subsequently routed to different decoding paradigms. For visual comprehension or pure text generation, the model employs a standard AR language modeling objective. For image generation, the continuous visual hidden states $\mathbf{Z}_s^{(t)}$, which have been integrated with the text instructions or descriptions $\mathbf{z}_{text}^{(t)}$, are decoded via our cascaded flow matching head.

Cascaded Flow Matching Head. Inspired by [43, 41, 44], we propose to explicitly decouple high-frequency visual details from low-frequency semantic features and then integrate them during image synthesis. Specifically, our CFM head consists of two cascaded stages, comprising 7 and 3 DiT blocks [7] respectively. Both stages employ the AdaLN-Zero [7] architecture to incorporate temporal modulations of the denoising procedure from the timestep t . In the first stage, the CFM head takes the contextualized hidden states $\mathbf{Z}_s^{(t)} \in \mathbb{R}^{h/2 \times w/2 \times c}$ from the LLM as input to perform low-resolution semantic generation. This is followed by a PixelShuffle [45] module that up-samples the feature maps to $2 \times$ resolution and low-dimension ones $\mathbf{Z}'_s^{(t)} \in \mathbb{R}^{h \times w \times d'}$. In the second stage, given the high-frequency patch details $S(D(\mathbf{z}_t)) \in \mathbb{R}^{h \times w \times d'}$, we first introduce a gating network $G(\cdot)$ to adaptively control the injection of fine-grained information to update the decoded features $\mathbf{Z}'_s^{(t)}$ as

$$\mathbf{Z}'_s^{(t)} \leftarrow G(\mathbf{Z}'_s^{(t)}) \odot S(D(\mathbf{z}_t)) + \mathbf{Z}'_s^{(t)},$$

where $G(\mathbf{Z}'_s^{(t)}) \in \mathbb{R}^{h \times w \times 1}$ denotes a scalar map and \odot the element-wise multiplication. Notably, as $\mathbf{Z}'_s^{(t)}$ is modulated by the timestep t in the first stage, the intensity of high-frequency injection (HFI) is dynamically coupled with the generative trajectory. Our empirical analysis (see section 3.3) reveals that, even without explicit supervision, the magnitude of HFI naturally intensifies as t progresses.

Finally, $\mathbf{Z}'_s^{(t)}$ is fed into subsequent DiT layers to predict the velocity field \mathbf{V}_t . Such a progression mirrors the hierarchical nature of human drawing, which naturally transitions from global layout sketching to localized detail refinement.

2.2 Inference and Training Objectives

Inference. For text-only and multimodal understanding tasks, we follow standard autoregressive decoding by sequentially selecting tokens from the predicted distribution. For image generation, we perform continuous-time flow-based

Table 1: Training setup and hyperparameters across different stages for CHEERS.

Stage	Vision-Language Alignment	General Pre-Training	Refined Pre-Training	Supervised Fine-Tuning
Dataset	Image caption Text-to-image	Pure text corpus Detailed image caption Text-to-image OCR data	Pure text corpus Synthetic generation data General VQA	Pure text corpus Instruction text-to-image High-quality instruction data
Learning rate	$1e^{-4}$	$1e^{-4}$	$4e^{-5}$	$2e^{-5}$
Training parts	Projection & CFM Head & Gate	All parameters w/o VAE	All parameters w/o VAE	All parameters w/o VAE
Schedules	constant	constant	constant	cosine
Batch size	512	512	512	128
Training steps	30 K	60 K	65 K	30 K

sampling starting from Gaussian noise in the latent space, denoted as \mathbf{z}_0 . At each time step t , we feed the current latent variable \mathbf{z}_t into the unified vision tokenizer to obtain the corresponding visual tokens, which are then jointly processed with the textual condition by the LLM. Subsequently, the CFM head predicts the continuous-time velocity field \mathbf{V}_t based on the LLM outputs, and we update the latent state via numerical integration:

$$\mathbf{z}_{t+\Delta t} = \mathbf{z}_t + \int_t^{t+\Delta t} \mathbf{V}_\tau d\tau.$$

The updated latent variable $\mathbf{z}_{t+\Delta t}$ serves as the input to the next integration step. By repeatedly applying tokenization, conditional modeling with the LLM, velocity prediction through the CFM Head, and numerical ODE integration, the latent trajectory is evolved from \mathbf{z}_0 to the terminal state \mathbf{z}_1 . The final latent \mathbf{z}_1 is then decoded using the VAE decoder to produce the output image.

In addition, following prior work [21], we adopt classifier-free guidance (CFG) during generation. To further adjust the time noise schedule in flow-based sampling, we apply a schedule shift and rescale the continuous-time variable with a hyperparameter α . Formally, given the original time step $t \in [0, 1]$, the shifted time step is computed as $\tilde{t} = \frac{\alpha t}{1+(\alpha-1)t}$.

Training Objectives. We use an end-to-end unified training optimization. For visual comprehension or pure text generation, the probability of generating the target text sequence $\mathbf{y} = \{y_1, \dots, y_L\}$ is factorized as $P_\theta(\mathbf{y}|\mathbf{C}) = \prod_{i=1}^L p_\theta(y_i|\mathbf{y}_{<i}, \mathbf{C})$, where \mathbf{C} represents the conditioning context, i.e., $[\mathbf{Z}_s^{(t)}]$ for image caption, $[\mathbf{Z}_s^{(t)}, \mathbf{Z}_{text}]$ for image question-answer or prefix $[\mathbf{Z}_{text}]$ for pure text. We use the standard cross-entropy loss function $\mathcal{L}_{AR} = -\log P_\theta(\mathbf{y}|\mathbf{C})$, where \mathbf{y} is the generated target text sequence, \mathbf{C} is the conditioning context, and θ are the learnable parameters of the model. For the image generation part, we use the flow matching loss function $\mathcal{L}_{FM} = \|v_\theta(\mathbf{Z}_s^{(t)}) - (\mathbf{z}_1 - \mathbf{z}_0)\|_2^2$. The overall training loss is the weighted sum of the text loss and image generation loss, given by:

$$\mathcal{L}_{total} = \mathcal{L}_{AR} + \lambda \mathcal{L}_{FM}$$

where λ is a hyperparameter used to balance the loss between text generation and image generation, and in our training, λ is set to 1.

2.3 Training Pipeline

Our four-stage progressive training is detailed in table 1. Image resolution is fixed at 512×512 . We initialize the image encoder from Siglip2 and FLUX.2. All experiments use the AdamW optimizer with a 0.02 warmup ratio and 1.0 gradient clipping, conducted on 128 NVIDIA A100 GPUs (16 nodes).

Stage I: Vision–Language Alignment. We train only the randomly initialized modules (projector, CFM head, and gating modules). The training data consists of 4.5M image-caption pairs from the LLaVA-UHD-v3 [46] and 1.3M ImageNet samples re-annotated by Qwen2.5-VL-3B [1]. To establish preliminary generative capability, we repeat the ImageNet dataset 10 times.

Stage II: General Pre-Training. Subsequently, we optimize all model parameters except the VAE using 30M multimodal samples. Understanding data comprises captions from Infinity-MM [47], LLaVA-UHD-v3 [46], and TextAtlas5M [48]. Generation data, including pretraining data from BLIP-3o [49], and a small portion of synthetic data re-generated using FLUX.2-klein-9B [6] with prompts from DiffusionDB [50]. Pure text data extracted from LLaVA-UHD-v3 [46]. The ratio of understanding, generation, and text data is 3 : 6 : 1.

Stage III: Refined Pre-Training. We focus on visual reasoning and semantic alignment using 33M samples in this stage, maintaining a 3 : 6 : 1 ratio across understanding, generation, and text data. We combine LLaVA-UHD-v3

Table 2: Evaluation on multimodal understanding benchmarks. #Params.: LLM backbone parameters.

Model	#Params.	General			OCR		Visual Spatial		Knowledge		
		SEEDBench	MMStar	MMBench	ChartQA	OCRBench	RealWorldQA	POPE	AI2D	MathVista	MMMU
<i>Understanding Only</i>											
MobileVLM-V2 [69]	1.4B	-	-	57.7	-	-	-	84.3	-	-	-
Qwen2-VL [70]	2B	-	48.0	72.2	73.5	80.9	62.9	-	74.7	43.0	41.1
DeepSeek-VL [71]	7B	70.4	-	73.2	-	45.6	-	88.1	-	36.1	36.6
mPLUG-Owl2 [72]	7B	57.8	-	64.5	22.8	25.5	50.3	86.2	55.7	-	32.7
<i>Understanding & Generation</i>											
Emu3 [30]	8B	68.2	-	58.5	<u>68.6</u>	68.7	<u>57.4</u>	85.2	<u>70.0</u>	-	31.6
Show-o [32]	1.3B	51.5	-	-	-	-	-	80.0	-	-	26.7
Show-o2 [21]	1.5B	65.6	<u>43.4</u>	67.4	40.0	24.5	56.5	-	69.0	-	<u>37.1</u>
JanusFlow [73]	1.3B	<u>70.5</u>	40.6	<u>74.9</u>	64.6	53.2	41.2	<u>88.0</u>	54.2	-	29.3
Janus-Pro [35]	1.5B	<u>68.3</u>	43.1	75.5	23.4	48.7	52.6	86.2	64.5	-	36.3
Harmon [74]	1.5B	67.1	35.3	65.5	29.8	11.2	49.8	87.6	57.0	-	38.9
Tar [75]	1.5B	70.4	-	65.6	-	-	-	88.4	-	-	36.0
CHEERS	1.5B	71.7	50.9	70.4	75.7	<u>58.4</u>	60.9	87.9	74.4	50.5	36.0

instruction data [46] for understanding and synthetic data generated via FLUX.2-klein-9B [6], utilizing prompts from DiffusionDB [50] and LLaVA-OneVision-1.5 [51]. To improve compositional reasoning (e.g., counting, color, and space), we also produced 466K instructions based on Objects365 [52] to synthesize images. Pure text data is extracted from Nemotron-Cascade [53].

Stage IV: Supervised Fine-Tuning. We fine-tune the model on 3.8M curated samples, incorporating a high-quality subset of the Stage III data with Echo-4o-Image [54], MoviePosters [55], and ShareGPT-4o-Image [56]. During training, we maintain a 1 : 1 batch ratio between understanding and generation tasks.

3 Experiments

We evaluate CHEERS on diverse multimodal benchmarks. We first describe the setup in section 3.1 and report main results in section 3.2. Subsequent analyses include visualizations in section 3.3, ablation studies in section 3.4, and an in-depth discussion of the model’s characteristics and limitations.

3.1 Evaluation Setup

Multimodal Understanding. We evaluate CHEERS on diverse and widely recognized multimodal understanding benchmarks. (1) General Benchmarks: SEEDBench [57], MMStar [58], MMBench [59]. (2) OCR Benchmarks: ChartQA [60], OCRBench [61]. (3) Visual Spatial Benchmarks: RealWorldQA [62], POPE [63]. (4) Knowledge-focused Benchmarks: AI2D [64], MathVista [65], MMMU [66].

Visual Generation. We evaluate visual generation performance on GenEval [67] and DPG-Bench [68]. GenEval is an object-focused evaluation framework designed to rigorously assess the compositional alignment and fine-grained controllable generation capabilities of text-to-image models. DPG-Bench is a comprehensive benchmark comprising over a thousand dense prompts designed to evaluate the semantic alignment and prompt-following capabilities of text-to-image models in complex, multi-entity scenarios.

3.2 Main Results

Image Understanding. As shown in table 2, CHEERS achieves competitive performance on nearly all benchmarks, demonstrating its strong and reliable understanding ability.

Image Generation. The results are summarized in table 3 and table 4. Across all benchmarks, CHEERS consistently achieves competitive or superior performance compared with existing approaches under comparable parameter scales, including models such as Janus-Pro. Notably, CHEERS attains these strong results using only 83M training samples in total, demonstrating that high-quality generation does not rely solely on large-scale data. This highlights the effectiveness of our unified architecture, whose shared representation design enables efficient knowledge transfer between understanding and generation, resulting in robust image synthesis performance with high data efficiency.

Progressive Improvement of Generation Capability. To illustrate how the generation capability of CHEERS evolves throughout training, we present the progression of GenEval scores across different stages in fig. 4. As shown in the figure, the model exhibits steady improvement as training proceeds, with clear performance gains at each stage. During

Table 3: Performances on GenEval. Obj.: Object; Attr.: Attribute; #Params.: LLM backbone parameters; #Data: total training samples (visual, image, and text).

Model	#Params.	#Data	Single Obj.	Two Obj.	Counting	Colors	Position	Color Attr.	Overall
<i>Generation Only</i>									
LlamaGen [76]	0.8B	62M	0.71	0.34	0.21	0.58	0.07	0.04	0.32
SDXL [77]	2.6B	-	0.98	0.74	0.39	0.85	0.15	0.23	0.55
DALL-E 3 [78]	-	-	0.96	0.87	0.47	0.83	0.43	0.45	0.67
SD3-Medium [79]	2B	-	0.99	0.94	0.72	0.89	0.33	0.60	0.74
<i>Understanding & Generation</i>									
Chameleon [18]	7B	5.2B	-	-	-	-	-	-	0.39
Show-o [32]	1.3B	3.2B	0.95	0.52	0.49	0.82	0.11	0.28	0.53
TokenFlow-XL [37]	14B	5.76B	0.95	0.60	0.41	0.81	0.16	0.24	0.55
Janus [34]	1.3B	-	0.97	0.68	0.30	0.84	0.46	0.42	0.61
JanusFlow [73]	1.3B	-	-	-	-	-	-	-	0.63
Transfusion [17]	7.3B	3.5B	-	-	-	-	-	-	0.63
D-DiT [80]	2B	40M	0.97	0.80	0.54	0.76	0.32	0.50	0.65
Emu3 [30]	8B	-	0.99	0.81	0.42	0.80	0.49	0.45	0.66
Janus-Pro [35]	1.5B	162M	0.98	0.82	0.51	0.89	0.65	0.56	0.73
Show-o2 [21]	1.5B	177M	0.99	0.86	0.55	0.86	0.46	0.63	0.73
Harmon [74]	1.5B	113M	0.99	0.86	0.66	0.85	0.74	0.48	0.76
Tar [75]	1.5B	403M	0.99	0.91	0.76	0.81	0.57	0.51	0.76
CHEERS	1.5B	83M	0.98	0.92	0.65	0.86	0.63	0.65	0.78

Table 4: Performances on DPG-Bench. #Params.: LLM backbone parameters; #Data: total training samples (visual, image, and text).

Model	#Params.	#Data	Global	Entity	Attribute	Relation	Other	Overall
<i>Generation Only</i>								
SDXL [77]	2.6B	-	83.27	82.43	80.91	86.76	80.41	74.65
DALL-E 3 [78]	-	-	90.97	89.61	88.39	90.58	89.83	83.50
SD3-Medium [79]	2B	-	87.90	91.01	88.83	80.70	88.68	84.08
<i>Understanding & Generation</i>								
JanusFlow [73]	1.3B	-	87.03	87.31	87.39	89.79	88.10	80.09
Emu3 [30]	8B	-	85.21	86.68	86.84	90.22	83.15	80.60
Janus-Pro [35]	1.5B	162M	87.58	88.63	88.17	88.98	88.30	82.63
Show-o2 [21]	1.5B	177M	87.53	90.38	91.34	90.30	91.21	85.02
Tar [75]	1.5B	403M	83.59	89.35	86.91	93.50	80.80	82.96
CHEERS	1.5B	83M	90.84	90.24	89.42	89.71	87.37	<u>83.48</u>

the Vision-Language Alignment and General Pre-Training stages, most of the generation training data consists of real-world natural images paired with captions. Such data are complex and ambiguous, as real-world scenes often contain multiple objects, intricate interactions, and incompletely described visual details, making it difficult for the model to learn precise text-to-image correspondences. As a result, although the model gradually acquires fundamental visual semantic understanding during these stages, the generation performance improves moderately and remains sub-optimal until a significant surge in the Refined Pre-Training stage, where the generation training data are primarily synthetic and instruction-oriented. Compared with real-world data, synthetic data provides clearer object compositions, more explicit attribute bindings, and more direct text-image correspondence, making the learning objective better defined and easier to optimize. This significantly enhances generation fidelity and alignment, leading to rapid improvement in generation ability. Finally, during Supervised Fine-Tuning, we adopt a smaller learning rate together with a cosine decay schedule to stabilize optimization, reduce overfitting, and encourage smoother convergence. This stage further refines output quality and alignment consistency, yielding stable and incremental performance gains. Overall, these results demonstrate that the generation capability of CHEERS improves in a progressive manner, validating the effectiveness of our staged training pipeline.



Figure 4: Overall training pipeline and the progression of the GenEval score. The curve above illustrates the GenEval score as a function of cumulative training steps.

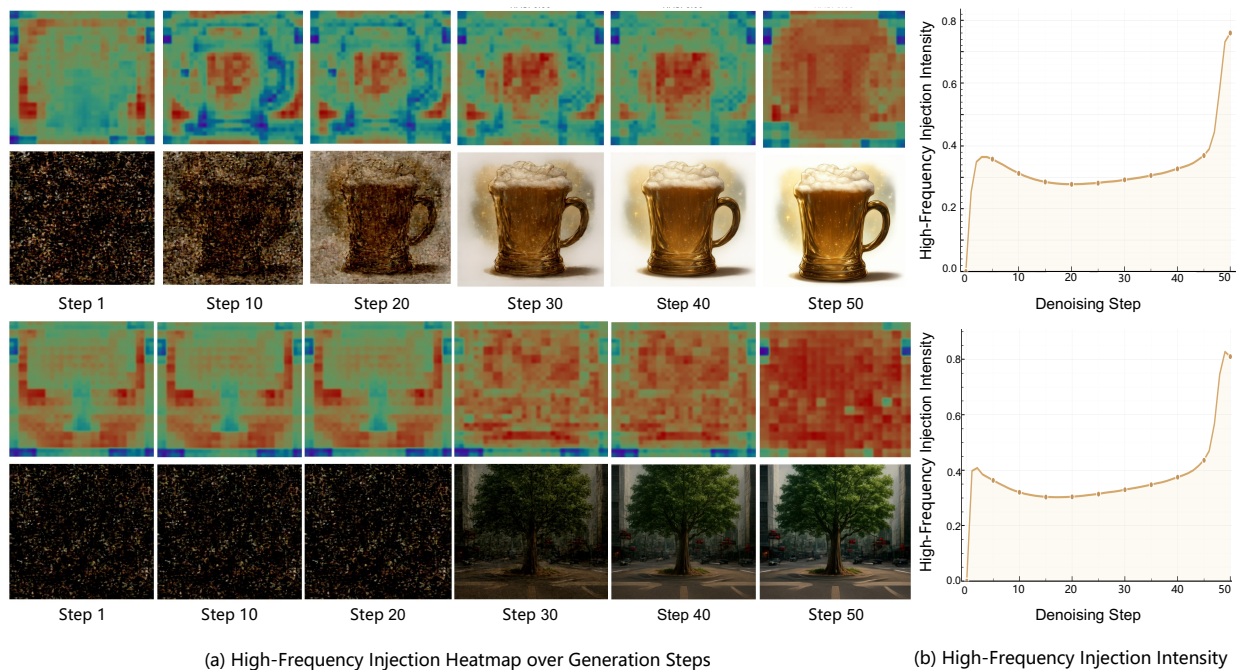


Figure 5: (a) Heatmap of high frequency injection across different generation steps. (b) High frequency injection intensity at each step. The reported values are aggregated over multiple runs, with per-run normalization applied prior to averaging across samples at the same step, ensuring a faithful representation of the overall trend.

3.3 Analysis of High-Frequency Injection

To investigate how high-frequency information contributes throughout the generation process, we visualize the high-frequency injection patterns across different denoising steps, as shown in fig. 5 (a). The heatmaps reveal a clear temporal structure. At the early stage of generation, high-frequency components are sparsely activated and mainly concentrate around the formation of the primary object contours. As generation progresses to the intermediate stage, the magnitude of HFI slightly decreases, and the model relies primarily on semantic and low-frequency signals to complete structural details and object-level compositions. In the final stage, when the overall image structure has largely stabilized, the activation of high-frequency components increases significantly, contributing to the refinement of local textures and

Table 5: Ablation results. The first row corresponds to a model fine-tuned using understanding data only. The second and third rows report jointly trained models optimized for both understanding and generation, without and with HFI, respectively.

Model	HFI	Fine-tuning Data	SEEDBench	MMBench	ChartQA	POPE	AI2D	GenEval	DPG-Bench
CHEERS	✓	Understanding	70.8	65.2	58.5	87.0	67.7	-	-
CHEERS	✗	Generation & Understanding	70.0	66.3	58.8	86.2	67.3	0.17	39.11
CHEERS	✓	Generation & Understanding	69.8	67.1	59.9	87.5	68.1	0.30	51.63

fine-grained visual details. This stage-wise evolution suggests that high-frequency signals are not uniformly involved, but instead dynamically modulated according to the generation stage.

fig. 5 (b) further quantifies the degree of high-frequency participation across the entire denoising trajectory. At the beginning of generation, the model focuses on constructing coarse layouts and global structures, during which HFI starts from a relatively low level. In the middle phase, semantic and low-frequency information guide the generation of object-level structures and attributes, resulting in a relatively moderate level of high-frequency participation. As the process approaches the final stages, the intensity and proportion of HFI increase sharply, indicating its growing role in enhancing local textures and visual fidelity. Such a progressive pattern reflects a hierarchical generation mechanism, where the model first sketches global layouts and semantic structures before gradually refining localized details and textures, resembling the coarse-to-fine process commonly observed in human drawing behavior.

3.4 Ablation Studies

We conduct controlled ablation experiments to investigate HFI and the impact of the generation objective on multimodal understanding. After standard Vision–Language Alignment, models are fine-tuned using 858K understanding and 850K generation samples (randomly sampled from Refined Pre-Training) for preliminary investigation and rapid validation.

Does Generation Affect Understanding? To further examine whether jointly training understanding and generation tasks under this architecture compromises multimodal understanding performance, we conduct a controlled experiment. After completing the alignment stage, we fine-tune a model using only multimodal understanding data as a baseline for comparison. The results, summarized in table 5, show that joint training with both understanding and generation objectives not only equips the model with image generation capability, but also achieves comparable or even slightly superior understanding performance compared to fine-tuning on understanding data alone. These findings demonstrate the effectiveness of the unified vision tokenizer design in supporting multimodal tasks within a single framework.

Is High-Frequency Injection Necessary? As shown in table 5, we train two models under identical training settings: CHEERS and a variant without HFI. The results indicate that introducing high-frequency patch details has minimal impact on multimodal understanding performance, while leading to a substantial improvement in generation quality. Although the model without HFI is able to produce semantically consistent images, the generated results lack fine-grained visual details. In contrast, incorporating high-frequency patch details significantly enhances texture fidelity and structural sharpness. These findings suggest that HFI plays a crucial role in improving visual detail generation, making it an essential component for unified multimodal modeling.

3.5 Discussion

CHEERS directly leverages the pre-trained weights of a native ViT model (e.g., SigLIP2), allowing the model to fully benefit from the rich representations learned during pre-training. In this way, we avoid the computational overhead of training a unified vision encoder, which has long been considered a key step in prior work for achieving unified vision-language understanding and generation. Moreover, our architecture does not freeze any core parameters, enabling all modules to be jointly fine-tuned. This ensures maximal synergy among components and allows the model to fully exploit the strengths of each module.

4 Related Work

4.1 Image Tokenizers.

Unified Multimodal Models (UMMs) necessitate a versatile visual representation capable of bridging the gap between discriminative understanding and generative synthesis. The design of image tokenizers is central to this objective, revolving around the trade-offs between representation formats, feature granularities, and architectural integration.

Discrete vs. Continuous Representations. The choice of tokenization dictates the modeling paradigm. Discrete tokenizers like Chameleon [18] map images to a finite codebook to leverage autoregressive objectives, yet often suffer from information bottlenecks and reduced fidelity. In contrast, continuous representations in KL-regularized latent spaces preserve richer details, becoming the preference for high-fidelity generation. As highlighted in TUNA [22], continuous features, when aligned with pretrained encoders, exhibit superior efficacy for both generative and semantic understanding tasks.

Semantic Features vs. High-Frequency Textures. A fundamental disparity exists between low-frequency semantics for reasoning and high-frequency textures for reconstruction. Semantic encoders like SigLIP [25] often overlook fine-grained textures, leading to blurred synthesis, while generative VAEs lack global context. To reconcile this, Show-o [32] explores late-fusion strategies, while TUNA [22] proposes a cascaded architecture that extracts semantics directly from VAE latents to achieve a balanced and unified representation space.

Unified visual tokenizer. Recent efforts focus on native unification. Discrete approaches like UniTok [81] and TokLIP [82] attempt to learn shared codebooks for dual tasks but remain constrained by discretization limits. Conversely, continuous unified frameworks integrate representation encoders with generative spaces. For instance, RAE [5, 83] leverages frozen semantic features for reconstruction, while TAR [12] and SVG [84] explore joint modeling. However, achieving a seamless balance between high-level reasoning and pixel-perfect generation remains a core challenge in UMM design.

4.2 Unified Multimodal Models.

Unified Multimodal Models (UMMs) represent a paradigm shift toward native architectural integration, aiming to bridge the structural divide between multimodal perception and generative synthesis within a shared transformer backbone. Current research can be broadly categorized into three primary paradigms based on their modeling objectives: pure autoregressive (AR), pure diffusion, and hybrid frameworks. Pure AR models, exemplified by Chameleon [18], Emu3 [30], and Janus-Pro [35], unify modalities by quantizing visual data into discrete token sequences and optimizing via the next-token prediction objective. This approach allows them to inherit the proven scaling laws and reasoning capabilities of large language models. Conversely, pure diffusion-based UMMs such as MMaDA [85] and UniDisc [86] adopt unified masked token prediction or stochastic denoising. These models benefit from parallel decoding efficiency, which achieves significantly higher inference speeds than sequential AR, and support bidirectional reasoning for tasks like joint image-text inpainting. Finally, hybrid architectures strategically fuse these mechanisms to maximize cross-modal synergy. Models like Show-o [32], Transfusion [17], and SEED-X [87] typically maintain autoregressive modeling for sequential language while employing diffusion or flow-matching processes for continuous visual representations, thereby achieving high-fidelity generation without compromising linguistic logic.

4.3 Synergy in Multimodal Comprehension and Generation.

The bidirectional synergy between multimodal comprehension and generation has become a pivotal research focus. Recent studies demonstrate that discriminative understanding significantly benefits generative performance. Specifically, REPA [88] aligns diffusion transformer features with pretrained visual encoders to accelerate convergence, while VA-VAE [27] addresses the optimization dilemma between reconstruction and generation by aligning latent spaces with vision foundation models. Conversely, generative tasks increasingly serve to bolster visual comprehension. ROSS [89] introduces a reconstructive objective via latent denoising to enhance fine-grained perception and reduce hallucinations. Furthermore, UniMRG [90] incorporates auxiliary generation of intrinsic representations such as depth and segmentation to capture geometric and structural cues. These advancements suggest that internalizing generative tasks allows unified models to develop a more comprehensive understanding of spatial relations and structural layouts.

5 Conclusion

In this work, we present CHEERS, a novel unified multimodal model that successfully harmonizes visual comprehension and high-fidelity generation within a single framework. The core of our approach lies in the decoupling of patch-level details from semantic representations, addressing the intrinsic optimization conflict that often plagues joint multimodal modeling. By utilizing a unified vision tokenizer to extract stable semantics and a cascaded flow matching head to inject semantically gated high-frequency residuals, CHEERS ensures both robust understanding and precise image synthesis. Extensive evaluations across ten understanding benchmarks and multiple generation benchmarks demonstrate that CHEERS achieves competitive performance. Notably, our model maintains high efficiency through a $4\times$ token compression rate and shows the emergence of zero-shot image editing capabilities, despite being trained on a relatively modest dataset of 83M samples. These results validate that the hierarchical progression from global semantic layout to

localized detail refinement—resembling the human drawing process—is an effective paradigm for unified modeling. While CHEERS exhibits strong performance, future research could explore further scaling of both the LLM backbone and training data to unlock even more complex reasoning and creative generation abilities. Additionally, extending this decoupled representation framework to video understanding and generation presents a promising avenue for achieving more generalized multimodal intelligence.

Limitation. Despite its performance, our study has three primary constraints. First, the relatively small parameter scale of CHEERS may limit its ability to capture intricate details. Second, as it is not initialized from large-scale pre-trained VLMs, its inherent visual understanding and generation capabilities require further enhancement. Finally, the current training pipeline relies on single-image datasets; future work will incorporate more diverse and complex multimodal data to improve generalization.

References

- [1] Shuai Bai, Keqin Chen, Xuejing Liu, Jialin Wang, Wenbin Ge, Sibao Song, Kai Dang, Peng Wang, Shijie Wang, Jun Tang, et al. Qwen2. 5-vl technical report. *arXiv preprint arXiv:2502.13923*, 2025.
- [2] Weiyun Wang, Zhangwei Gao, Lixin Gu, Hengjun Pu, Long Cui, Xingguang Wei, Zhaoyang Liu, Linglin Jing, Shenglong Ye, Jie Shao, et al. Internvl3. 5: Advancing open-source multimodal models in versatility, reasoning, and efficiency. *arXiv preprint arXiv:2508.18265*, 2025.
- [3] Boqiang Zhang, Kehan Li, Zesen Cheng, Zhiqiang Hu, Yuqian Yuan, Guanzheng Chen, Sicong Leng, Yuming Jiang, Hang Zhang, Xin Li, et al. Videollama 3: Frontier multimodal foundation models for image and video understanding. *arXiv preprint arXiv:2501.13106*, 2025.
- [4] Kimi Team, Tongtong Bai, Yifan Bai, Yiping Bao, SH Cai, Yuan Cao, Y Charles, HS Che, Cheng Chen, Guanduo Chen, et al. Kimi k2. 5: Visual agentic intelligence. *arXiv preprint arXiv:2602.02276*, 2026.
- [5] Boyang Zheng, Nanye Ma, Shengbang Tong, and Saining Xie. Diffusion transformers with representation autoencoders. *arXiv preprint arXiv:2510.11690*, 2025.
- [6] Black Forest Labs. FLUX.2: Frontier Visual Intelligence. <https://bf1.ai/blog/flux-2>, 2025.
- [7] William Peebles and Saining Xie. Scalable diffusion models with transformers. *arXiv preprint arXiv:2212.09748*, 2022.
- [8] Robin Rombach, Andreas Blattmann, Dominik Lorenz, Patrick Esser, and Björn Ommer. High-resolution image synthesis with latent diffusion models, 2021.
- [9] Shanchuan Lin, Anran Wang, and Xiao Yang. Sdxl-lightning: Progressive adversarial diffusion distillation. *arXiv preprint arXiv:2402.13929*, 2024.
- [10] Black Forest Labs, Stephen Batifol, Andreas Blattmann, Frederic Boesel, Saksham Consul, Cyril Diagne, Tim Dockhorn, Jack English, Zion English, Patrick Esser, Sumith Kulal, Kyle Lacey, Yam Levi, Cheng Li, Dominik Lorenz, Jonas Müller, Dustin Podell, Robin Rombach, Harry Saini, Axel Sauer, and Luke Smith. Flux.1 kontext: Flow matching for in-context image generation and editing in latent space, 2025.
- [11] Aaron Van Den Oord, Oriol Vinyals, et al. Neural discrete representation learning. *Advances in neural information processing systems*, 30, 2017.
- [12] Jiaming Han, Hao Chen, Yang Zhao, Hanyu Wang, Qi Zhao, Ziyan Yang, Hao He, Xiangyu Yue, and Lu Jiang. Vision as a dialect: Unifying visual understanding and generation via text-aligned representations. *arXiv preprint arXiv:2506.18898*, 2025.
- [13] Keyu Tian, Yi Jiang, Zehuan Yuan, Bingyue Peng, and Liwei Wang. Visual autoregressive modeling: Scalable image generation via next-scale prediction. *Advances in neural information processing systems*, 37:84839–84865, 2024.
- [14] Seungdae Han and Joohee Kim. Clip-vqdiffusion: Language free training of text to image generation using clip and vector quantized diffusion model. *arXiv preprint arXiv:2403.14944*, 2024.
- [15] Wei Song, Yuran Wang, Zijia Song, Yadong Li, Haoze Sun, Weipeng Chen, Zenan Zhou, Jianhua Xu, Jiaqi Wang, and Kaicheng Yu. Dualtoken: Towards unifying visual understanding and generation with dual visual vocabularies. *arXiv preprint arXiv:2503.14324*, 2025.
- [16] Hao Liu, Wilson Yan, Matei Zaharia, and Pieter Abbeel. World model on million-length video and language with blockwise ringattention. *arXiv preprint arXiv:2402.08268*, 2024.

- [17] Chunting Zhou, Lili Yu, Arun Babu, Kushal Tirumala, Michihiro Yasunaga, Leonid Shamis, Jacob Kahn, Xuezhe Ma, Luke Zettlemoyer, and Omer Levy. Transfusion: Predict the next token and diffuse images with one multi-modal model. *arXiv preprint arXiv:2408.11039*, 2024.
- [18] Chameleon Team. Chameleon: Mixed-modal early-fusion foundation models. *arXiv preprint arXiv:2405.09818*, 2024.
- [19] Enze Xie, Junsong Chen, Junyu Chen, Han Cai, Haotian Tang, Yujun Lin, Zhekai Zhang, Muyang Li, Ligeng Zhu, Yao Lu, and Song Han. Sana: Efficient high-resolution image synthesis with linear diffusion transformer, 2024.
- [20] Jiayou Zhang, Yifan Shen, Guangyi Chen, Le Song, and Eric P Xing. Dimensional collapse in vqvae: Evidence and remedies. In *The Thirty-ninth Annual Conference on Neural Information Processing Systems*.
- [21] Jinheng Xie, Zhenheng Yang, and Mike Zheng Shou. Show-o2: Improved native unified multimodal models. *arXiv preprint arXiv:2506.15564*, 2025.
- [22] Zhiheng Liu, Weiming Ren, Haozhe Liu, Zijian Zhou, Shoufa Chen, Haonan Qiu, Xiaoke Huang, Zhaochong An, Fanny Yang, Aditya Patel, et al. Tuna: Taming unified visual representations for native unified multimodal models. *arXiv preprint arXiv:2512.02014*, 2025.
- [23] Chaorui Deng, Deyao Zhu, Kunchang Li, Chenhui Gou, Feng Li, Zeyu Wang, Shu Zhong, Weihao Yu, Xiaonan Nie, Ziang Song, et al. Emerging properties in unified multimodal pretraining. *arXiv preprint arXiv:2505.14683*, 2025.
- [24] Alec Radford, Jong Wook Kim, Chris Hallacy, Aditya Ramesh, Gabriel Goh, Sandhini Agarwal, Girish Sastry, Amanda Askell, Pamela Mishkin, Jack Clark, et al. Learning transferable visual models from natural language supervision. In *International conference on machine learning*, pages 8748–8763. PmLR, 2021.
- [25] Michael Tschanen, Alexey Gritsenko, Xiao Wang, Muhammad Ferjad Naeem, Ibrahim Alabdulmohsin, Nikhil Parthasarathy, Talfan Evans, Lucas Beyer, Ye Xia, Basil Mustafa, et al. Siglip 2: Multilingual vision-language encoders with improved semantic understanding, localization, and dense features. *arXiv preprint arXiv:2502.14786*, 2025.
- [26] Diederik P Kingma and Max Welling. Auto-encoding variational bayes. *arXiv preprint arXiv:1312.6114*, 2013.
- [27] Jingfeng Yao, Bin Yang, and Xinggang Wang. Reconstruction vs. generation: Taming optimization dilemma in latent diffusion models. In *Proceedings of the Computer Vision and Pattern Recognition Conference*, pages 15703–15712, 2025.
- [28] Quan Sun, Qiyong Yu, Yufeng Cui, Fan Zhang, Xiaosong Zhang, Yueze Wang, Hongcheng Gao, Jingjing Liu, Tiejun Huang, and Xinlong Wang. Emu: Generative pretraining in multimodality. *arXiv preprint arXiv:2307.05222*, 2023.
- [29] Quan Sun, Yufeng Cui, Xiaosong Zhang, Fan Zhang, Qiyong Yu, Yueze Wang, Yongming Rao, Jingjing Liu, Tiejun Huang, and Xinlong Wang. Generative multimodal models are in-context learners. In *Proceedings of the IEEE/CVF conference on computer vision and pattern recognition*, pages 14398–14409, 2024.
- [30] Xinlong Wang, Xiaosong Zhang, Zhengxiong Luo, Quan Sun, Yufeng Cui, Jinsheng Wang, Fan Zhang, Yueze Wang, Zhen Li, Qiyong Yu, et al. Emu3: Next-token prediction is all you need. *arXiv preprint arXiv:2409.18869*, 2024.
- [31] Yufeng Cui, Honghao Chen, Haoge Deng, Xu Huang, Xinghang Li, Jirong Liu, Yang Liu, Zhuoyan Luo, Jinsheng Wang, Wenxuan Wang, et al. Emu3. 5: Native multimodal models are world learners. *arXiv preprint arXiv:2510.26583*, 2025.
- [32] Jinheng Xie, Weijia Mao, Zechen Bai, David Junhao Zhang, Weihao Wang, Kevin Qinghong Lin, Yuchao Gu, Zhijie Chen, Zhenheng Yang, and Mike Zheng Shou. Show-o: One single transformer to unify multimodal understanding and generation. *arXiv preprint arXiv:2408.12528*, 2024.
- [33] NextStep Team, Chunrui Han, Guopeng Li, Jingwei Wu, Quan Sun, Yan Cai, Yuang Peng, Zheng Ge, Deyu Zhou, Haomiao Tang, et al. Nextstep-1: Toward autoregressive image generation with continuous tokens at scale. *arXiv preprint arXiv:2508.10711*, 2025.
- [34] Chengyue Wu, Xiaokang Chen, Zhiyu Wu, Yiyang Ma, Xingchao Liu, Zizheng Pan, Wen Liu, Zhenda Xie, Xingkai Yu, Chong Ruan, et al. Janus: Decoupling visual encoding for unified multimodal understanding and generation. *arXiv preprint arXiv:2410.13848*, 2024.
- [35] Xiaokang Chen, Zhiyu Wu, Xingchao Liu, Zizheng Pan, Wen Liu, Zhenda Xie, Xingkai Yu, and Chong Ruan. Janus-pro: Unified multimodal understanding and generation with data and model scaling. *arXiv preprint arXiv:2501.17811*, 2025.

- [36] Chao Liao, Liyang Liu, Xun Wang, Zhengxiong Luo, Xinyu Zhang, Wenliang Zhao, Jie Wu, Liang Li, Zhi Tian, and Weilin Huang. Mogao: An omni foundation model for interleaved multi-modal generation. *arXiv preprint arXiv:2505.05472*, 2025.
- [37] Liao Qu, Huichao Zhang, Yiheng Liu, Xu Wang, Yi Jiang, Yiming Gao, Hu Ye, Daniel K Du, Zehuan Yuan, and Xinglong Wu. Tokenflow: Unified image tokenizer for multimodal understanding and generation. In *Proceedings of the Computer Vision and Pattern Recognition Conference*, pages 2545–2555, 2025.
- [38] Yecheng Wu, Zhuoyang Zhang, Junyu Chen, Haotian Tang, Dacheng Li, Yunhao Fang, Ligeng Zhu, Enze Xie, Hongxu Yin, Li Yi, et al. Vila-u: a unified foundation model integrating visual understanding and generation. *arXiv preprint arXiv:2409.04429*, 2024.
- [39] Jingfeng Yao, Yuda Song, Yucong Zhou, and Xinggong Wang. Towards scalable pre-training of visual tokenizers for generation. *arXiv preprint arXiv:2512.13687*, 2025.
- [40] Sinan Du, Jiahao Guo, Bo Li, Shuhao Cui, Zhengzhuo Xu, Yifu Luo, Yongxian Wei, Kun Gai, Xinggong Wang, Kai Wu, et al. Vqrae: Representation quantization autoencoders for multimodal understanding, generation and reconstruction. *arXiv preprint arXiv:2511.23386*, 2025.
- [41] Alan Baade, Eric Ryan Chan, Kyle Sargent, Changan Chen, Justin Johnson, Ehsan Adeli, and Li Fei-Fei. Latent forcing: Reordering the diffusion trajectory for pixel-space image generation. *arXiv preprint arXiv:2602.11401*, 2026.
- [42] Qwen Team. Qwen2.5: A party of foundation models, September 2024.
- [43] Weichen Fan, Haiwen Diao, Quan Wang, Dahua Lin, and Ziwei Liu. The prism hypothesis: Harmonizing semantic and pixel representations via unified autoencoding. *arXiv preprint arXiv:2512.19693*, 2025.
- [44] Fengjiao Chen, Minhao Jing, Weitao Lu, Yan Feng, Xiaoyu Li, and Xuezhi Cao. Unihetero: Could generation enhance understanding for vision-language-model at large data scale? *arXiv preprint arXiv:2512.23512*, 2025.
- [45] Wenzhe Shi, Jose Caballero, Ferenc Huszár, Johannes Totz, Andrew P Aitken, Rob Bishop, Daniel Rueckert, and Zehan Wang. Real-time single image and video super-resolution using an efficient sub-pixel convolutional neural network. In *Proceedings of the IEEE conference on computer vision and pattern recognition*, pages 1874–1883, 2016.
- [46] Shichu Sun, Yichen Zhang, Haolin Song, Zonghao Guo, Chi Chen, Yidan Zhang, Yuan Yao, Zhiyuan Liu, and Maosong Sun. Llava-uhd v3: Progressive visual compression for efficient native-resolution encoding in mllms. *arXiv preprint arXiv:2511.21150*, 2025.
- [47] Shuhao Gu, Jialing Zhang, Siyuan Zhou, Kevin Yu, Zhaohu Xing, Liangdong Wang, Zhou Cao, Jintao Jia, Zhuoyi Zhang, Yixuan Wang, et al. Infinity-mm: Scaling multimodal performance with large-scale and high-quality instruction data. *arXiv preprint arXiv:2410.18558*, 2024.
- [48] Alex Jinpeng Wang, Dongxing Mao, Jiawei Zhang, Weiming Han, Zhuobai Dong, Linjie Li, Yiqi Lin, Zhengyuan Yang, Libo Qin, Fuwei Zhang, et al. Textatlas5m: A large-scale dataset for dense text image generation. *arXiv preprint arXiv:2502.07870*, 2025.
- [49] Jiuhai Chen, Zhiyang Xu, Xichen Pan, Yushi Hu, Can Qin, Tom Goldstein, Lifu Huang, Tianyi Zhou, Saining Xie, Silvio Savarese, et al. Blip3-o: A family of fully open unified multimodal models-architecture, training and dataset. *arXiv preprint arXiv:2505.09568*, 2025.
- [50] Zijie J Wang, Evan Montoya, David Munechika, Haoyang Yang, Benjamin Hoover, and Duen Horng Chau. Diffusiondb: A large-scale prompt gallery dataset for text-to-image generative models. In *Proceedings of the 61st annual meeting of the association for computational linguistics (volume 1: Long papers)*, pages 893–911, 2023.
- [51] Xiang An, Yin Xie, Kaicheng Yang, Wenkang Zhang, Xiuwei Zhao, Zheng Cheng, Yirui Wang, Songcen Xu, Changrui Chen, Chunsheng Wu, Huajie Tan, Chunyuan Li, Jing Yang, Jie Yu, Xiyao Wang, Bin Qin, Yumeng Wang, Zizhen Yan, Ziyong Feng, Ziwei Liu, Bo Li, and Jiankang Deng. Llava-onevision-1.5: Fully open framework for democratized multimodal training, 2025.
- [52] Shuai Shao, Zeming Li, Tianyuan Zhang, Chao Peng, Gang Yu, Xiangyu Zhang, Jing Li, and Jian Sun. Objects365: A large-scale, high-quality dataset for object detection. In *Proceedings of the IEEE/CVF international conference on computer vision*, pages 8430–8439, 2019.
- [53] Boxin Wang, Chankyu Lee, Nayeon Lee, Sheng-Chieh Lin, Wenliang Dai, Yang Chen, Yangyi Chen, Zhuolin Yang, Zihan Liu, Mohammad Shoeybi, et al. Nemotron-cascade: Scaling cascaded reinforcement learning for general-purpose reasoning models. *arXiv preprint arXiv:2512.13607*, 2025.
- [54] Junyan Ye, Dongzhi Jiang, Zihao Wang, Leqi Zhu, Zhenghao Hu, Zilong Huang, Jun He, Zhiyuan Yan, Jinghua Yu, Hongsheng Li, et al. Echo-4o: Harnessing the power of gpt-4o synthetic images for improved image generation. *arXiv preprint arXiv:2508.09987*, 2025.

- [55] skvarre. movie-posters-100k. https://huggingface.co/datasets/skvarre/movie_posters-100k, 2023.
- [56] Junying Chen, Zhenyang Cai, Pengcheng Chen, Shunian Chen, Ke Ji, Xidong Wang, Yunjin Yang, and Benyou Wang. Sharept-4o-image: Aligning multimodal models with gpt-4o-level image generation. *arXiv preprint arXiv:2506.18095*, 2025.
- [57] Bohao Li, Rui Wang, Guangzhi Wang, Yuying Ge, Yixiao Ge, and Ying Shan. Seed-bench: Benchmarking multimodal llms with generative comprehension. *arXiv preprint arXiv:2307.16125*, 2023.
- [58] Lin Chen, Jinsong Li, Xiaoyi Dong, Pan Zhang, Yuhang Zang, Zehui Chen, Haodong Duan, Jiaqi Wang, Yu Qiao, Dahua Lin, et al. Are we on the right way for evaluating large vision-language models? *Advances in Neural Information Processing Systems*, 37:27056–27087, 2024.
- [59] Yuan Liu, Haodong Duan, Yuanhan Zhang, Bo Li, Songyang Zhang, Wangbo Zhao, Yike Yuan, Jiaqi Wang, Conghui He, Ziwei Liu, et al. Mmbench: Is your multi-modal model an all-around player? In *European conference on computer vision*, pages 216–233. Springer, 2024.
- [60] Ahmed Masry, Xuan Long Do, Jia Qing Tan, Shafiq Joty, and Enamul Hoque. Chartqa: A benchmark for question answering about charts with visual and logical reasoning. In *Findings of the association for computational linguistics: ACL 2022*, pages 2263–2279, 2022.
- [61] Yuliang Liu, Zhang Li, Mingxin Huang, Biao Yang, Wenwen Yu, Chunyuan Li, Xu-Cheng Yin, Cheng-Lin Liu, Lianwen Jin, and Xiang Bai. Ocrbench: on the hidden mystery of ocr in large multimodal models. *Science China Information Sciences*, 67(12):220102, 2024.
- [62] X.AI. Grok-1.5 vision preview. <https://x.ai/blog/grok-1.5v>, 2024.
- [63] Yifan Li, Yifan Du, Kun Zhou, Jinpeng Wang, Wayne Xin Zhao, and Ji-Rong Wen. Evaluating object hallucination in large vision-language models. In *Proceedings of the 2023 conference on empirical methods in natural language processing*, pages 292–305, 2023.
- [64] Aniruddha Kembhavi, Mike Salvato, Eric Kolve, Minjoon Seo, Hannaneh Hajishirzi, and Ali Farhadi. A diagram is worth a dozen images. In *European conference on computer vision*, pages 235–251. Springer, 2016.
- [65] Pan Lu, Hritik Bansal, Tony Xia, Jiacheng Liu, Chunyuan Li, Hannaneh Hajishirzi, Hao Cheng, Kai-Wei Chang, Michel Galley, and Jianfeng Gao. Mathvista: Evaluating mathematical reasoning of foundation models in visual contexts. *arXiv preprint arXiv:2310.02255*, 2023.
- [66] Xiang Yue, Yuansheng Ni, Kai Zhang, Tianyu Zheng, Ruoqi Liu, Ge Zhang, Samuel Stevens, Dongfu Jiang, Weiming Ren, Yuxuan Sun, et al. Mmmu: A massive multi-discipline multimodal understanding and reasoning benchmark for expert agi. In *Proceedings of the IEEE/CVF conference on computer vision and pattern recognition*, pages 9556–9567, 2024.
- [67] Dhruva Ghosh, Hannaneh Hajishirzi, and Ludwig Schmidt. Geneval: An object-focused framework for evaluating text-to-image alignment. *Advances in Neural Information Processing Systems*, 36:52132–52152, 2023.
- [68] Xiwei Hu, Rui Wang, Yixiao Fang, Bin Fu, Pei Cheng, and Gang Yu. Ella: Equip diffusion models with llm for enhanced semantic alignment. *arXiv preprint arXiv:2403.05135*, 2024.
- [69] Xiangxiang Chu, Limeng Qiao, Xinyu Zhang, Shuang Xu, Fei Wei, Yang Yang, Xiaofei Sun, Yiming Hu, Xinyang Lin, Bo Zhang, et al. Mobilevlm v2: Faster and stronger baseline for vision language model. *arXiv preprint arXiv:2402.03766*, 2024.
- [70] Peng Wang, Shuai Bai, Sinan Tan, Shijie Wang, Zhihao Fan, Jinze Bai, Keqin Chen, Xuejing Liu, Jialin Wang, Wenbin Ge, et al. Qwen2-vl: Enhancing vision-language model’s perception of the world at any resolution. *arXiv preprint arXiv:2409.12191*, 2024.
- [71] Haoyu Lu, Wen Liu, Bo Zhang, Bingxuan Wang, Kai Dong, Bo Liu, Jingxiang Sun, Tongzheng Ren, Zhuoshu Li, Hao Yang, et al. Deepseek-vl: towards real-world vision-language understanding. *arXiv preprint arXiv:2403.05525*, 2024.
- [72] Qinghao Ye, Haiyang Xu, Jiabo Ye, Ming Yan, Anwen Hu, Haowei Liu, Qi Qian, Ji Zhang, and Fei Huang. mplug-owl2: Revolutionizing multi-modal large language model with modality collaboration. In *Proceedings of the IEEE/CVF conference on computer vision and pattern recognition*, pages 13040–13051, 2024.
- [73] Yiyang Ma, Xingchao Liu, Xiaokang Chen, Wen Liu, Chengyue Wu, Zhiyu Wu, Zizheng Pan, Zhenda Xie, Haowei Zhang, Xingkai Yu, et al. Janusflow: Harmonizing autoregression and rectified flow for unified multimodal understanding and generation. In *Proceedings of the IEEE/CVF Conference on Computer Vision and Pattern Recognition*, pages 7739–7751, 2025.

- [74] Size Wu, Wenwei Zhang, Lumin Xu, Sheng Jin, Zhonghua Wu, Qingyi Tao, Wentao Liu, Wei Li, and Chen Change Loy. Harmonizing visual representations for unified multimodal understanding and generation. In *Proceedings of the IEEE/CVF International Conference on Computer Vision*, pages 17739–17750, 2025.
- [75] Jiaming Han, Hao Chen, Yang Zhao, Hanyu Wang, Qi Zhao, Ziyang Yang, Hao He, Xiangyu Yue, and Lu Jiang. Vision as a dialect: Unifying visual understanding and generation via text-aligned representations. *arXiv preprint arXiv:2506.18898*, 2025.
- [76] Peize Sun, Yi Jiang, Shoufa Chen, Shilong Zhang, Bingyue Peng, Ping Luo, and Zehuan Yuan. Autoregressive model beats diffusion: Llama for scalable image generation. *arXiv preprint arXiv:2406.06525*, 2024.
- [77] Dustin Podell, Zion English, Kyle Lacey, Andreas Blattmann, Tim Dockhorn, Jonas Müller, Joe Penna, and Robin Rombach. Sdxl: Improving latent diffusion models for high-resolution image synthesis. *arXiv preprint arXiv:2307.01952*, 2023.
- [78] James Betker, Gabriel Goh, Li Jing, Tim Brooks, Jianfeng Wang, Linjie Li, Long Ouyang, Juntang Zhuang, Joyce Lee, Yufei Guo, et al. Improving image generation with better captions. *Computer Science*. <https://cdn.openai.com/papers/dall-e-3.pdf>, 2(3):8, 2023.
- [79] Patrick Esser, Sumith Kulal, Andreas Blattmann, Rahim Entezari, Jonas Müller, Harry Saini, Yam Levi, Dominik Lorenz, Axel Sauer, Frederic Boesel, et al. Scaling rectified flow transformers for high-resolution image synthesis. In *Forty-first international conference on machine learning*, 2024.
- [80] Zijie Li, Henry Li, Yichun Shi, Amir Barati Farimani, Yuval Kluger, Linjie Yang, and Peng Wang. Dual diffusion for unified image generation and understanding. In *Proceedings of the Computer Vision and Pattern Recognition Conference*, pages 2779–2790, 2025.
- [81] Chuofan Ma, Yi Jiang, Junfeng Wu, Jihan Yang, Xin Yu, Zehuan Yuan, Bingyue Peng, and Xiaojuan Qi. Unitok: A unified tokenizer for visual generation and understanding. *arXiv preprint arXiv:2502.20321*, 2025.
- [82] Haokun Lin, Teng Wang, Yixiao Ge, Yuying Ge, Zhichao Lu, Ying Wei, Qingfu Zhang, Zhenan Sun, and Ying Shan. Toklip: Marry visual tokens to clip for multimodal comprehension and generation. *arXiv preprint arXiv:2505.05422*, 2025.
- [83] Shengbang Tong, Boyang Zheng, Ziteng Wang, Bingda Tang, Nanye Ma, Ellis Brown, Jihan Yang, Rob Fergus, Yann LeCun, and Saining Xie. Scaling text-to-image diffusion transformers with representation autoencoders. *arXiv preprint arXiv:2601.16208*, 2026.
- [84] Minglei Shi, Haolin Wang, Wenzhao Zheng, Ziyang Yuan, Xiaoshi Wu, Xintao Wang, Pengfei Wan, Jie Zhou, and Jiwen Lu. Latent diffusion model without variational autoencoder. *arXiv preprint arXiv:2510.15301*, 2025.
- [85] Ling Yang, Ye Tian, Bowen Li, Xinchen Zhang, Ke Shen, Yunhai Tong, and Mengdi Wang. Mmada: Multimodal large diffusion language models. *arXiv preprint arXiv:2505.15809*, 2025.
- [86] Alexander Swerdlow, Mihir Prabhudesai, Siddharth Gandhi, Deepak Pathak, and Katerina Fragkiadaki. Unified multimodal discrete diffusion. *arXiv preprint arXiv:2503.20853*, 2025.
- [87] Yuying Ge, Sijie Zhao, Jinguo Zhu, Yixiao Ge, Kun Yi, Lin Song, Chen Li, Xiaohan Ding, and Ying Shan. Seed-x: Multimodal models with unified multi-granularity comprehension and generation. *arXiv preprint arXiv:2404.14396*, 2024.
- [88] Sihyun Yu, Sangkyung Kwak, Huiwon Jang, Jongheon Jeong, Jonathan Huang, Jinwoo Shin, and Saining Xie. Representation alignment for generation: Training diffusion transformers is easier than you think. *arXiv preprint arXiv:2410.06940*, 2024.
- [89] Haochen Wang, Anlin Zheng, Yucheng Zhao, Tiancai Wang, Zheng Ge, Xiangyu Zhang, and Zhaoxiang Zhang. Reconstructive visual instruction tuning. *arXiv preprint arXiv:2410.09575*, 2024.
- [90] Zihan Su, Hongyang Wei, Kangrui Cen, Yong Wang, Guanhua Chen, Chun Yuan, and Xiangxiang Chu. Generation enhances understanding in unified multimodal models via multi-representation generation. *arXiv preprint arXiv:2601.21406*, 2026.

A Why Reconstruct Pixels Before Semantic Encoding?

Table 6: Effect of Pixel-Reconstruct on OCR-centric understanding and Others. We scale the alignment dataset from 558K to 4.6M samples (both fine-tuned on the same 858K data) to ensure sufficient training, and then introduce Pixel-Reconstruct under the same 4.6M alignment setting for comparison.

Model	Pixel-Reconstruct	Training Data	ChartQA	OCRBench	TextVQA	MMBench	MMStar	SEEDBench
CHEERS	✗	558K & 858K	13.9	2.5	9.6	23.2	27.7	38.4
CHEERS	✗	4.6M & 858K	14.2	2.2	9.5	42.8	32.1	56.9
CHEERS (Ours)	✓	558K & 858K	42.1	31.5	43.4	66.09	40.2	69.2

In our initial design, the latent representation produced by the VAE encoder was directly projected and fed into the SigLIP2-ViT for semantic encoding. However, preliminary experiments revealed that this design leads to severe degradation in OCR-centric understanding ability. Here we conducted a controlled study to analyze this issue.

All experiments in this section are conducted at a resolution of 256×256 , focusing only on evaluating the model’s visual understanding capability. The first two rows in Table 6 follow the design adopted in TUNA, where the latent representation from the VAE encoder is directly processed by a ViT backbone without using a VAE decoder. Under this setting, the model exhibits extremely poor performance on OCR-related benchmarks, indicating that fine-grained textual information is largely lost. To verify whether this issue stems from insufficient training data, we further scale the alignment dataset to 4.6M samples while keeping the same 858K fine-tuning set. As shown in the second row of Table 6, increasing the training data brings negligible improvement on OCR-related benchmarks, suggesting that the performance degradation is not caused by insufficient data but rather by the architectural design.

To address this issue, we introduce a VAE decoder that reconstructs the latent representation back into the pixel space before semantic encoding. The reconstructed image is then processed by the SigLIP2-ViT to extract semantic tokens. As shown in the third row of Table 6, introducing the reconstruction stage leads to substantial improvements across OCR-centric benchmarks. These results indicate that reconstructing pixels before semantic encoding is necessary for preserving fine-grained visual details that are crucial for text recognition.

B Emergent Abilities

To investigate the advantages of our Unified Visual Tokenizer in learning a shared feature space, we evaluate the checkpoint after Stage 3 training and observe several intriguing emergent capabilities. Notably, throughout all training stages up to Stage 3, the generation training only involves text-to-image tasks, without exposure to any multi-image or image editing data.

As show in table 7, despite not being trained on any image editing or multi-image data, CHEERS still demonstrates remarkable potential on these tasks. This observation highlights the strong generalization ability of the proposed framework. In particular, the unified visual tokenizer enables different visual tasks to be represented within a shared feature space, which naturally facilitates capability transfer across tasks. These results further validate the effectiveness of learning a unified visual representation.

C Examples of Multimodal Understanding

The main paper reports the quantitative performance of CHEERS on multimodal understanding tasks. To further illustrate its capabilities, we present several qualitative examples in table 8. These cases demonstrate that CHEERS is able to effectively comprehend and reason over multimodal inputs, exhibiting strong multimodal understanding ability. For multimodal understanding, input images are resized so that the longer side is 512 pixels while preserving the aspect ratio, and then padded to a resolution of 512×512 before being fed into the model.

Table 7: Emergent capabilities of CHEERS after Refined Pre-Training.

Change the color of the background to blue.



Turn this apple into a watermelon.



Place the red bell pepper from Figure 1 and the green broccoli from Figure 2 into one image.



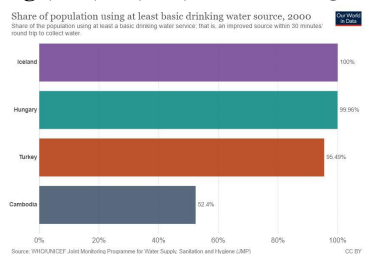
Table 8: Emergent capabilities of CHEERS after Refined Pre-Training.

Discribe this image.



This image captures a cozy corner of a room with a stunning view of the ocean. The foreground features a stone wall with a wooden ceiling, creating a warm and rustic atmosphere. A black chair is tucked under a small table, which holds a vase with red flowers and a framed picture. A large window dominates the scene, offering an impressive view of the sea and distant land. The ocean stretches out to the horizon, meeting a clear blue sky. In the distance, a city skyline and mountains can be seen, adding depth and interest to the landscape. Inside the room, a straw-like hanging lamp adds a touch of texture and soft lighting. A potted palm tree adds a tropical feel to the space. The overall scene is serene and inviting, with a perfect blend of natural and man-made elements. It's a peaceful coastal retreat that combines comfort with a breathtaking view.

Please answer the question requiring a floating-point number with one decimal place and provide the final value, e.g. , 1.2, 1.3, 1.4, at the end. Question: What is the difference of largest and smallest bar?



To find the difference between the largest and smallest bar, we need to identify the values of the largest and smallest bars from the given data. The largest bar represents Iceland, with a value of 100.0. The smallest bar represents Cambodia, with a value of 52.4. Now, we need to calculate the difference between these two values: $100.0 - 52.4 = 47.6$. Therefore, the difference between the largest and smallest bar is 47.6.